Research Article Vol. 59, No. 12 / 20 April 2020 / Applied Optics 3589

applied optics

Schlieren masks: square root monomials, sigmoidal functions, and off-axis Gaussians

CRISTINA M. GÓMEZ-SARABIA[1] AND JORGE OJEDA-CASTAÑEDA[2,*]

[1]Digital Arts, Engineering Division, University of Guanajuato, Carretera a Valle, Salamanca 36885, Mexico
[2]Electronics Department, Engineering Division, University of Guanajuato, Carretera a Valle, Salamanca 36885, Mexico
*Corresponding author: jojedacas@ugto.mx

Received 2 January 2020; accepted 19 March 2020; posted 23 March 2020 (Doc. ID 387370); published 16 April 2020

By using an effective transfer function, one can describe conveniently the nonlinear mapping between an input thin transparent structure and its image irradiance distribution. This effective transfer function is useful for making sound comparisons between several spatial filters employed for phase rendering. Here, we unveil three nonconventional Schlieren techniques, which employ absorption masks whose amplitude distributions are described by square root monomials, by sigmoidal functions, or by off-axis Gaussian functions. We apply the effective transfer function for analyzing the similarities between the proposed masks and other Schlieren techniques.

https://doi.org/10.1364/AO.387370

1. INTRODUCTION

For several applications in microscopy, holography, and optical testing, it is extremely useful to be able to visualize, as image irradiance variations, the presence of transparent structures.

One can render visible the presence of phase-only variations by using suitable filtering masks, for example, dark background imagery [1], the Foucault knife-edge [2], Toepler [3], Kastler [4] and Wolter [5] edge techniques, the amplitude modulation technique [6], the Lyot test [7], and Zernike's phase contrast method [8]. An interesting square root technique has been reported [9].

It is not so well known that an effective transfer function can describe the mapping from a thin transparent structure into image irradiance distributions [10–13]. This effective transfer function is useful for analyzing and classifying several spatial filters as members of the Schlieren techniques [14,15].

On the other hand, Jacquinot coined the word apodization for describing the use of spatial filters that reduce the sidelobes of the impulse response [16]. As a secondary effect, apodization spatial filters broaden the central lobe of the impulse response [17,18]. It is relevant to note that by reducing the sidelobes and widening the central lobe, classical apodizers can be applied for broadening the axial impulse response, and therefore for extending focal depth [19–21].

Here, our aim is to unveil the use of three nonconventional Schlieren techniques, whose amplitude distributions are described by square root monomials, by sigmoidal functions, or by off-axis Gaussian mask. These masks are able to render visible phase variations with apodizing effects. We apply the effective transfer function for numerically evaluating the characteristics of our proposals and for analyzing their similarities with other Schlieren techniques.

For the sake of completeness of our proposal, in Section 2, we briefly revisit the basics of the effective transfer function. For the sake of clarity of our description, we use as input pattern a thin phase, sinusoidal grating. In Section 3, we discuss the use of three nonconventional masks for rendering visible these phase variations. We report numerical graphs and novel formulas describing the effective transfer functions. In Section 4, we analyze the similarities of our proposed masks with other Schlieren techniques. In Section 5, we summarize our contribution.

2. EFFECTIVE TRANSFER FUNCTION

In Fig. 1(a), we show schematically the use of a coherent optical processor for rendering visible phase structures. In what follows, we discuss a simple model for describing this type of image formation process.

To this end, we consider a 1D model, and we employ as the input transparency a thin phase, sinusoidal grating. For a generalization of the current simple approach, please see Refs. [12,13].

In mathematical terms, at the input plane, the complex amplitude distribution is

$$u_0(x) = \exp\left[i\,2\pi\left(\frac{a}{\lambda}\right)\,\sin\left(2\pi\frac{x}{d}\right)\right]. \tag{1}$$

In Eq. (1), the maximum value of the optical path difference is denoted with the lowercase, Latin letter a. The lowercase, Greek letter λ denotes the wavelength of the monochromatic

radiation. And, we represent the period of the phase grating with the lowercase, Latin letter d.

By assuming that the values of the optical path difference are very small as compared with λ, $a \ll \lambda$, the complex amplitude in Eq. (1) can be expressed as

$$u_1(x) = 1 + i\,2\pi\left(\frac{a}{\lambda}\right)\sin\left(2\pi\frac{x}{d}\right). \tag{2}$$

At the Fraunhofer plane, the complex amplitude distribution is obtained by taking the Fourier transform of Eq. (2), which is

$$U_1(\mu) = \delta(\mu) + \left(\pi\frac{a}{\lambda}\right)\left[-\delta\left(\mu + \frac{1}{d}\right) + \delta\left(\mu - \frac{1}{d}\right)\right]. \tag{3}$$

In Eq. (3), we use the lowercase Greek letter μ for denoting the spatial frequency, at the Fraunhofer plane. Just behind the spatial filter, located at the Fraunhofer plane, the complex amplitude distribution is

$$U_2(\mu) = P(\mu)\;\; U_1(\mu). \tag{4}$$

In Eq. (4), we denote the complex amplitude transmittance of the generalized pupil function as $P(\mu)$.

Hence, by combining Eqs. (3) and (4) and by taking the inverse Fourier transform of the resultant combination, we obtain the complex amplitude distribution at the image,

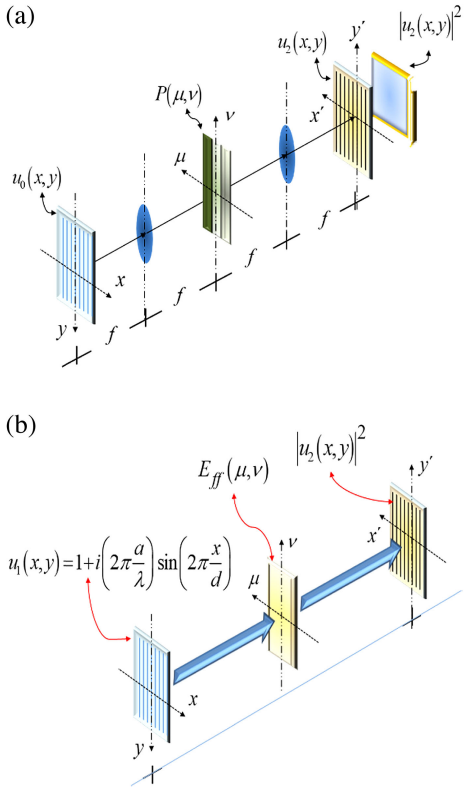

Fig. 1. Schematics of the optical setups for rendering visible transparent structures as image irradiance variations. In (a), we show a classical optical processor with an asymmetric mask at the Fraunhofer plane and a square law detector at the image plane. In (b), we depict the use of an effective transfer function, which describes conveniently the nonlinear mapping between thin phase variations and image irradiance variations.

$$u_2(x) = P(0) + \int_{-\infty}^{\infty} P(\mu)\,U_1(\mu)\exp(i\,2\pi x\mu)\,\mathrm{d}\mu. \tag{5}$$

Now, it is convenient to define the normalized irradiance distribution as

$$I(x) = \frac{|u_2(x)|^2}{|P(0)|^2}. \tag{6}$$

By substituting Eq. (5) in Eq. (6), we obtain

$$I(x) = 1 + \left(2\pi\frac{a}{\lambda}\right)\int_{-\infty}^{\infty} E_{ff}(\mu)\Psi(\mu)\exp(i\,2\pi x\mu)\mathrm{d}\mu. \tag{7}$$

In Eq. (7), we define the effective transfer function as

$$E_{ff}(\mu) = \frac{1}{|P(0)|^2}[P^*(0)\,P(\mu) - P(0)\,P^*(-\mu)]. \tag{8}$$

As depicted schematically in Fig. 1(b), the effective transfer function in Eq. (8) represents the nonlinear mapping (including the square law detector) from the input phase variations into the image irradiance distributions. In what follows, we apply the above useful formulation for unveiling the use of three nonconventional Schlieren techniques.

3. NOVEL SCHLIEREN MASKS

Schlieren techniques employ spatial filters that have asymmetrical, real transmittances. Consequently, the effective transfer function, in Eq. (8), describes the odd component of the asymmetrical function. In mathematical terms,

$$E_{ff}(\mu) = \frac{1}{|P(0)|}[P(\mu) - P(-\mu)]. \tag{9}$$

The result in Eq. (9) emphasizes that the effective transfer function is a scaled version of the odd part of the generalized pupil function $P(\mu)$.

In Fig. 2, we depict the usefulness of employing the effective transfer function, for making comparisons between related classical Schlieren techniques. The lines in red describe the amplitude transmittance of the Foucault knife-edge test.

In Fig. 2, we plot in blue a ramp function representing the amplitude transmittance of a mask with linear absorption.

And, also in Fig. 2, in black, we plot the amplitude transmittance of a high light throughput version of the amplitude modulation microscopy.

Now, for describing our current proposals, we consider the use of masks that have amplitude transmittances proportional to square root monomials, inside a rectangular pupil aperture. It is convenient to represent the variations inside the pupil by employing a rectangular window. We denote with the upper case, Greek letter Ω, the cutoff spatial frequency. Hence, the amplitude transmittance of the square root monomials reads

$$P_n(\mu) = \left|\left(\frac{\mu}{2\Omega} + \frac{1}{2}\right)\right|^{\frac{1}{2n}}\mathrm{rect}\left(\frac{\mu}{2\,\Omega}\right). \tag{10}$$

In Eq. (10), the lowercase, Latin letter n stands for a positive, integer number greater than or equal to unity.

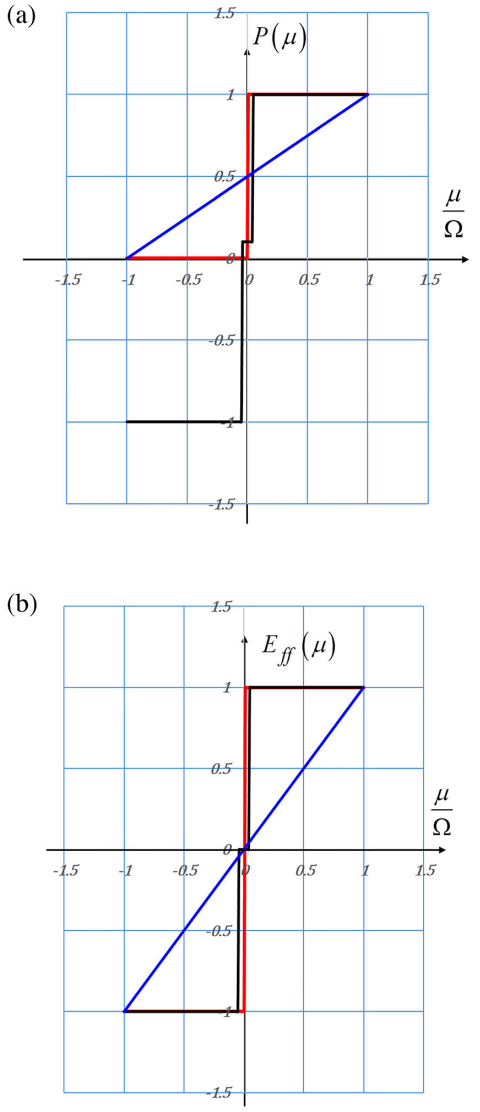

Fig. 2. Amplitude transmittance of the certain Schlieren techniques. In (a), we show the generalized pupil functions. In (b), we plot their related effective transfer functions.

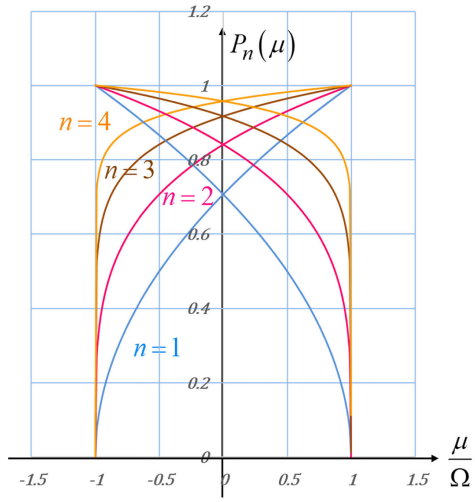

Fig. 3. Graphs depicting the amplitude transmittances of the square root monomials, $P_n(\mu)$ in Eq. (10), as well as the mirror symmetric functions $P_n(-\mu)$.

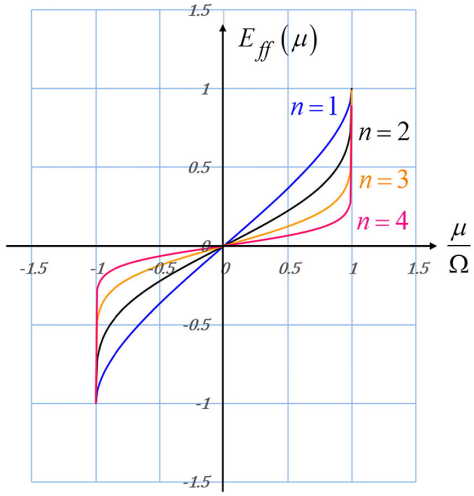

Fig. 4. The effective transfer functions generated by using the square root monomials in Eq. (10).

In Fig. 3, we plot the functions $P_n(\mu)$ as well as the functions $P_n(-\mu)$, for $n = 1, 2, 3, 4$.

In Fig. 4, we plot the amplitude transmittance of the effective transfer functions for this type of mask. It is apparent from Fig. 4 that the effective transfer works as a high frequency enhancer.

Specifically, for $n = 1$, the effective transfer function closely relates to the amplitude transmittance of a spatial filter implementing a first-order derivative.

Next, we consider absorption masks whose amplitude transmittance profile is a sigmoidal function,

$$P(\mu) = \frac{\exp\left[b\frac{\mu}{\Omega}\right]}{1+\exp\left[b\frac{\mu}{\Omega}\right]}\operatorname{rect}\left(\frac{\mu}{2\Omega}\right). \tag{11}$$

In Eq. (11), the lowercase Latin letter b denotes a dimensionless width parameter, which specifies the variation rate of the sigmoidal function.

In Fig. 5, we plot the amplitude transmittance of the pupil functions of the sigmoidal functions, for different values of the width parameter b.

Now, the effective transfer function reads

$$E_{ff}(\mu) = 4\frac{\sinh\left[b\frac{\mu}{\Omega}\right]}{1+\cosh\left[b\frac{\mu}{\Omega}\right]}\operatorname{rect}\left(\frac{\mu}{2\Omega}\right). \tag{12}$$

In Fig. 6, we plot the amplitude transmittance of the effective transfer function in Eq. (12), for different values of the dimensionless width parameter b.

It is apparent from Fig. 6 that as the value of the width parameter increases, then the effective transfer functions resemble those effective transfer functions associated to the Foucault knife-edge. However, due to smooth variations of the sigmoidal functions, one expects to obtain some apodizing effect on the image irradiance distributions.

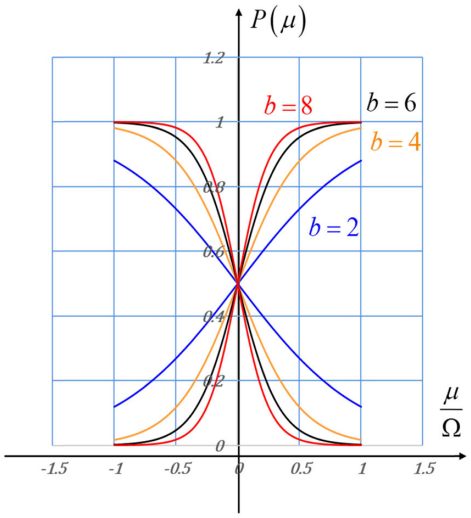

Fig. 5. Amplitude transmittances of the sigmoidal masks, $P(\mu)$ in Eq. (11), and the functions $P_n(-\mu)$, for several values of the width parameter b.

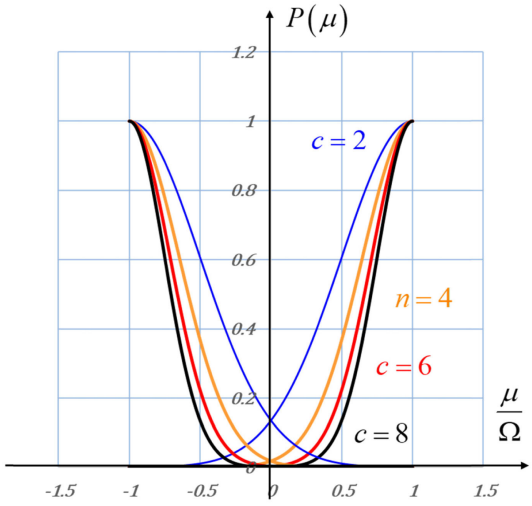

Fig. 7. Amplitude transmittances of the off-axis Gaussian functions, $P(\mu)$ in Eq. (13), as well as their mirror functions $P_n(-\mu)$, for several values of the half-width parameter c.

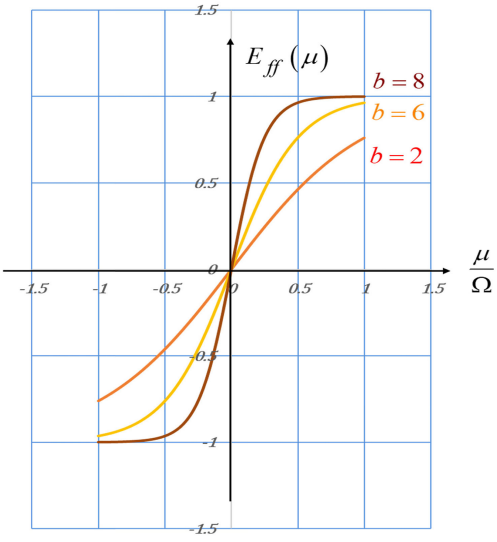

Fig. 6. Amplitude transmittance of the effective transfer function in Eq. (12) for the width parameter $b = 2$, 6, and 8.

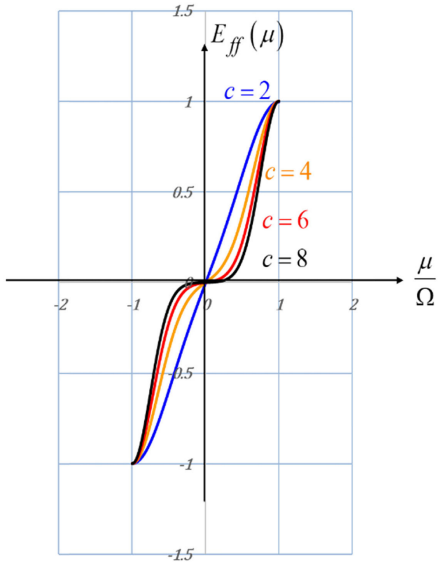

Fig. 8. Amplitude transmittance of the effective transfer function in Eq. (15).

Next, we consider absorption masks whose amplitude transmittance profile is an off-axis Gaussian function. For this case, the generalized pupil function is

$$P(\mu) = \exp\left[-c\left(\frac{\mu}{\Omega} - 1\right)^2\right] \operatorname{rect}\left(\frac{\mu}{2\,\Omega}\right). \tag{13}$$

In Eq. (13), the lowercase Latin letter c denotes a dimensionless parameter, which specifies the half-width of the Gaussian function. In Fig. 7, we plot the amplitude transmittance of the pupil functions of the off-axis Gaussian functions for different values of the half-width parameter c.

From Fig. 7, one can recognize that as the dimensionless factor increases, the off-axis Gaussians tend to attenuate the low frequency content.

For this type of mask, the effective transfer function reads

$$E_{ff}(\mu) = \exp\left[-2c\left(\frac{\mu}{\Omega}\right)^2\right] \sinh\left(2c\frac{\mu}{\Omega}\right) \operatorname{rect}\left(\frac{\mu}{2\,\Omega}\right). \tag{14}$$

In Fig. 8, we show the graphs of this type of effective transfer function.

It is apparent from Fig. 8 that as the value of the half-width parameter increases, the effective transfer functions reduce strongly the low frequency content of the phase structure.

Low values of the half-width parameter will be useful for obtaining an apodized version of Foucault knife-edge.

For relating our previous results in a succinct manner, we discuss the characteristics of a selection of the proposed masks.

4. RELEVANT COMPARISONS

For making useful comparisons, in Fig. 9, we plot the effective transfer functions of a sigmodal function with dimensionless parameter $b = 8$. And, in orange, we plot the effective transfer function of the off-axis Gaussian mask with dimensionless half-width $c = 2$.

Furthermore, in Fig. 9, we are showing also the effective transfer functions of a ramp function (in a continuous black line), as well as the effective transfer function of the Foucault knife-edge (in a broken black line).

We note that the sigmoidal function is good apodized version of the Foucault knife-edge. Hence, the sigmoidal function is here identified as the best choice between the current proposed masks.

For obtaining another viewpoint on this choice, in Fig. 10, we simulate numerically the irradiance distributions on the image

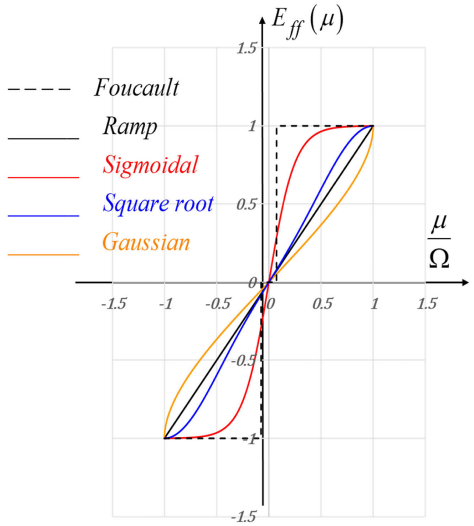

Fig. 9. Graphical comparisons of the effective transfer functions, which are generated by employing the proposed Schlieren masks.

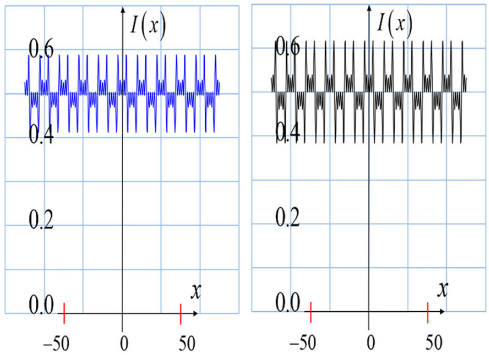

Fig. 10. Numerical simulations of the modulation variations, which are caused on the image irradiance by the square root mask (at the left-hand side, curve in blue) and by the ramp mask (at the right-hand side, curve in black).

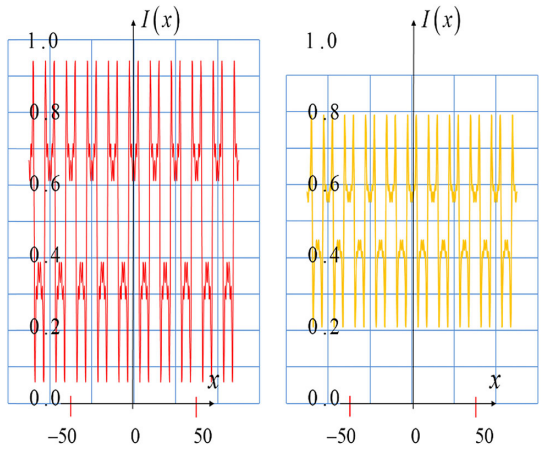

Fig. 11. Numerical simulations of the modulation variations, which are caused on the image irradiance by the sigmoidal mask (at the left-hand side, curve in red) and by the off-axis Gaussian mask (at the right-hand side, curve in orange).

of the thin phase grating. For our simulations, we assume that the spatial frequency of the grating $(1/d)$ is one-tenth of the value of the cutoff spatial frequency Ω.

At the left-hand side of Fig. 10, we show the irradiance variations.

At the left-hand side of Fig. 10, we show the irradiance variations (in blue) caused by using the square root monomial, with $n = 1$.

At the right-hand side of Fig. 10, we show the irradiance variations (in black) caused by using linear (ramp) absorption mask.

At the left-hand side of Fig. 11, we show the irradiance variations (in red) generated by the used a sigmoidal function with $b = 8$. And at the right-hand side of Fig. 11, we plot the irradiance variations (in orange) obtained by using an off-axis Gaussian mask with $c = 2$.

It is apparent from Figs. 10 and 11 that the image irradiance distributions have the highest possible modulation, when using the sigmoidal mask, with dimensionless parameter $b = 8$.

5. CONCLUDING REMARKS

We have employed an effective transfer function for describing the nonlinear mapping between an input thin transparent structure and its image irradiance distribution.

By using this mathematical tool, we have unveiled and analyzed three nonconventional Schlieren techniques. We have recommended the use of masks with sigmoidal amplitude variations, as a good choice for substituting with apodizing effects, and the classical knife-edge technique for rendering visible thin phase variations.

Disclosures. The authors declare that there are no conflicts of interest related to this paper.

REFERENCES

1. S. H. Gage, "Modern dark-field microscopy and the history of its development," Trans. Am. Microsc. Soc. **39**, 95–141 (1920).

2. L. Foucault, "Description des procédées employés pour reconnaitre la configuration des surfaces optiques," Comptes rendus hebdomadaires des séances de l'Académie des Sciences **47**, 958–959 (1858).
3. A. Toepler, "Beobachtungen Singender Flammenmit clem Schlierenapparat," Pogg. Ann. **128**, 126–845 (1866).
4. A. Kastler, "Un Systeme de franges de Diffraction a Grand Contraste," Rev. Opt. **29**, 307–412 (1950).
5. H. Wolter, "Schlieren-Phase Kontrast und Lichtschnittverfahren," in *Handbuch der Physik* (Springer, 1956), Vol. **24**, pp. 555–645.
6. R. Hoffman and L. Gross, "Modulation contrast microscope," Appl. Opt. **14**, 1169–1176 (1975).
7. B. Lyot, "Procedes Perme Hand d'Etudier les Irregularities d'une Surface Optique Bien Polie," C. R. Acad. Sci. **222**, 765 (1946).
8. F. Zernike, "Phase contrast, a new method for the microscopic observation of transparent objects," Physica **9**, 686–698 (1942).
9. B. A. Horwitz, "Phase image differentiation with linear intensity output," Appl. Opt. **17**, 181–186 (1978).
10. E. Menzel, "Die Darstellung verschiedener Phasekontrast Verfahren in der Optischen Ubertragungstheori," Optik (Stuttgart) **15**, 460–470 (1958).
11. E. Menzel, "Transfer-functions in optics," Optik (Stuttgart) **39**, 170–172 (1973).
12. J. Ojeda-Castaneda, "Necessary and sufficient conditions for thin phase imagery," Opt. Acta **27**, 905–915 (1980).
13. J. Ojeda-Castaneda, "A proposal to classify methods employed to detect thin phase structures under coherent illumination," Opt. Acta **27**, 917–929 (1980).
14. J. Ojeda-Castaneda and L. R. Berriel-Valdos, "Classification scheme and properties of schlieren techniques," Appl. Opt. **18**, 3338–3341 (1979).
15. J. Ojeda-Castaneda, "Foucault, wire, and phase modulation tests," in *Optical Shop Testing*, D. Malacara, ed. (Wiley, 2007), Chap. 8.
16. P. Jacquinot and B. Roizen-Dossier, "Apodisation," in *Progress in Optics*, E. Wolf, ed. (Elsevier, 1964), Vol. **3**, pp. 29–186.
17. W. H. Steel, *Interferometry*, 2 ed. (Cambridge University, 1986), pp. 234–235.
18. M. Ya Mints and E. D. Prilepskii, "Apodization of a passive optical system with aberrations," Opt. Spectrosc. **52**, 538–541 (1982).
19. J. Ojeda-Castaneda, L. R. Berriel-Valdos, and E. Montes, "Bessel annular apodizers: imaging characteristics," Appl. Opt. **26**, 2770–2772 (1987).
20. J. Ojeda-Castaneda, E. Tepichín, and A. Díaz, "Arbitrarily high focal depth with a quasi-optimum real and positive transmittance apodizers," Appl. Opt. **28**, 2666–2670 (1989).
21. J. Ojeda-Castaneda, P. Andres, and A. Diaz, "Annular apodizer for low sensitivity to defocus and to spherical aberration," Opt. Lett. **11**, 487–489 (1986).